Spontaneous formation of aligned DNA nanowires by capillarity-induced skin folding

So Nagashima[a,1], Hyun Dong Ha[a], Do Hyun Kim[a], Andrej Košmrlj[b], Howard A. Stone[b,2], and Myoung-Woon Moon[a,2]

[a]Materials and Life Science Research Division, Korea Institute of Science and Technology, Seoul 136-791, Republic of Korea; and [b]Department of Mechanical and Aerospace Engineering, Princeton University, Princeton, NJ 08544

Edited by Robert H. Austin, Princeton University, Princeton, NJ, and approved May 10, 2017 (received for review January 1, 2017)

Although DNA nanowires have proven useful as a template for fabricating functional nanomaterials and a platform for genetic analysis, their widespread use is still hindered because of limited control over the size, geometry, and alignment of the nanowires. Here, we document the capillarity-induced folding of an initially wrinkled surface and present an approach to the spontaneous formation of aligned DNA nanowires using a template whose surface morphology dynamically changes in response to liquid. In particular, we exploit the familiar wrinkling phenomenon that results from compression of a thin skin on a soft substrate. Once a droplet of liquid solution containing DNA molecules is placed on the wrinkled surface, the liquid from the droplet enters certain wrinkled channels. The capillary forces deform wrinkles containing liquid into sharp folds, whereas the neighboring empty wrinkles are stretched out. In this way, we obtain a periodic array of folded channels that contain liquid solution with DNA molecules. Such an approach serves as a template for the fabrication of arrays of straight or wrinkled DNA nanowires, where their characteristic scales are robustly tunable with the physical properties of liquid and the mechanical and geometrical properties of the elastic system.

DNA nanowires | capillary forces | wrinkling | folding | instability

Assembling biomolecules and microorganisms (e.g., virus and DNA) into a desired architecture has offered new routes to the fabrication of nanomaterials (1, 2). In particular, DNA nanowires have proven useful as a template to fabricate functional nanomaterials and as a platform for genetic analysis (3–5). Molecular combing and its derivatives have been used widely to obtain such nanowires using an aqueous solution of DNA molecules, where capillary forces of the solution at a receding meniscus act to stretch and immobilize the molecules on a solid surface (6). To manipulate the size, geometry, and alignment of nanowires, much effort has been devoted to controlling the evaporation of the solutions by adjusting experimental parameters, such as concentration and temperature, or applying external forces that move the droplets in a desired direction (7–9). However, these approaches require careful handling only to generate nanowires that are randomly positioned and oriented. Templates whose surfaces are decorated with patterns, such as microwells (10), nanogratings (11), and micropillars (12, 13), have been shown to guide the location of nanowires. However, the experimental approaches for creating such patterns largely rely on lithography-based methods, which involve complex processes that are not readily accessible.

Mechanical instabilities that occur in response to external stimuli (e.g., loading and heat) and geometric constraints cause surface wrinkling and folding of skin–substrate systems, which are ubiquitous in nature and have been harnessed to create wrinkled and folded materials for versatile applications (14). The transition from wrinkling to folding occurs when the mismatch compressive strain between the skin and substrate attains a critical value and has been exploited to develop functional materials and to rationalize morphogenetic features of biological systems (15–20). The wrinkle-to-fold transition is, however, difficult to achieve in practice because relatively large compressive strains need to be induced in the skin–substrate system (15, 17, 18, 21, 22). Addressing this limit would open up new opportunities for the development of advanced functional materials.

Here, we present an approach for the spontaneous formation of unidirectionally aligned DNA nanowires using a wrinkled skin–substrate template, which changes its surface morphology dynamically in response to water. In particular, we exploit capillary forces of water containing DNA molecules to trigger a wrinkle-to-fold transition of the template surface in an unconventional way, which in turn stretches and confines the molecules in a periodic array of folds without any external forces. This approach allows us to robustly control the size of DNA nanowires and manipulate their morphology between straight and undulating.

The template was prepared by oxygen plasma treatment of prestretched polydimethylsiloxane (PDMS) substrates for varying durations t, resulting in a skin–substrate system with a range of skin thicknesses. The nominal compressive strain ε induced in the skin was measured relative to the prestretched state of the substrate, and the magnitude of ε was controlled by adjustment of the release of the stretch. Unless otherwise noted, the contact angle θ of a droplet on the flat skin surface is $\theta \approx 5°$.

Results and Discussion

The spontaneous formation of DNA nanowires is illustrated in Fig. 1 *A* and *B*. When a droplet of water contacts a wrinkled skin, localized folds emerge at the boundary of the droplet, which is accompanied by spontaneous formation of water filaments that, in the case of a solution of DNA, help stretch and confine the molecules to the folds. While the droplet is spreading over the

Significance

Developing a method that is capable of manipulating the size, geometry, and alignment of DNA nanowires would expand their uses in fabricating functional materials and performing genetic analysis. Here, we present an approach that yields arrays of size-controllable straight or undulated DNA nanowires. This approach uses a template composed of a thin skin that dynamically changes its surface morphology in response to water. In particular, we exploit capillary forces of water containing DNA molecules to induce a wrinkle-to-fold transition of the template surface in an unconventional way, which in turn stretches and confines the molecules in the folded regions without any external forces and consequently forms the nanowires. This approach could make possible new fabrication opportunities for functional materials.

Author contributions: S.N., H.A.S., and M.-W.M. designed research; S.N., H.D.H., D.H.K., H.A.S., and M.-W.M. performed research; S.N., H.D.H., and A.K. analyzed data; and S.N., A.K., H.A.S., and M.-W.M. wrote the paper.

The authors declare no conflict of interest.

This article is a PNAS Direct Submission.

[1]Present address: Graduate School of Engineering, Osaka University, Suita 565-0871, Japan.

[2]To whom correspondence may be addressed. Email: hastone@Princeton.edu or mwmoon@kist.re.kr.

This article contains supporting information online at www.pnas.org/lookup/suppl/doi:10.1073/pnas.1700003114/-/DCSupplemental.

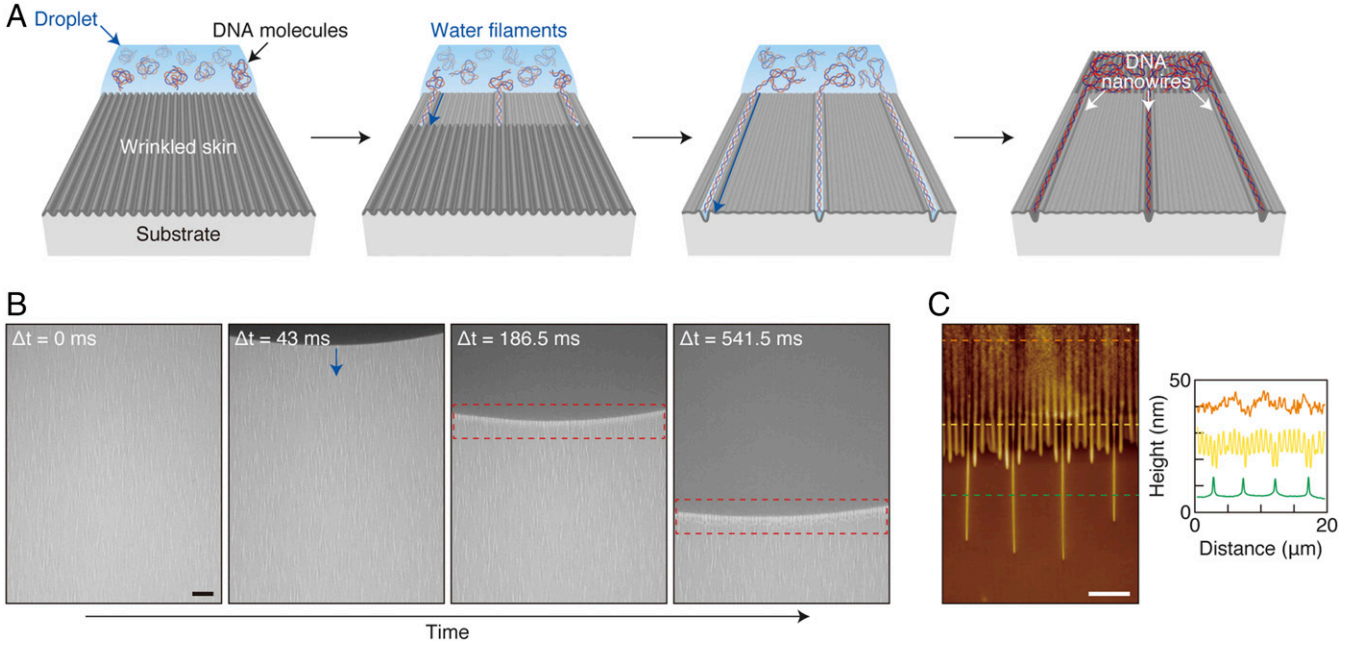

Fig. 1. Spontaneous formation of aligned DNA nanowires. (*A*) Schematic illustrations of the spontaneous formation of an array of DNA nanowires by the skin folding induced by water filaments containing DNA molecules. (*B*) Sequential optical microscope images of a droplet of DNA solution spreading over wrinkles (t = 5 min, $\varepsilon \approx -0.03$); the wrinkle-to-fold transition occurs at the boundary and propagates with the edge of the droplet. (*C*) AFM image of an array of DNA nanowires extending from the boundary (t = 2 min, $\varepsilon \approx -0.02$). The line profiles for each region are shown next to the image. (Scale bars: *B*, 50 μm and *C*, 4 μm.)

surface the folds continue to form at the boundary (red dotted boxes in Fig. 1*B*). Once the water evaporates, an array of DNA nanowires appears (Fig. 1*C*).

Here, we uncover a unique feature of the wrinkle-to-fold transition of the skin due to water. Upon deposition of a water droplet on a skin that has already been wrinkled due to small compressive strains, folds containing water filaments immediately appear around the boundary of droplet (Fig. 2*A* and Movie S1). The horizontal component $\gamma\cos\theta$ of the surface tension of water ($\gamma = 0.072$ N/m) pulls on the wrinkled skin and forms localized folds containing water, whereas the amplitude of the neighboring empty wrinkles is reduced (Fig. 2*B*). Note that when a droplet is placed on an initially flat uncompressed surface ($\varepsilon = 0.00$), the surface remains flat. However, once the skin is subsequently compressed by $\varepsilon \approx -0.01$, which is equivalent to the critical strain ε_c for surface wrinkling as described below, localized folds emerge around the droplet boundary (red triangles in Fig. 2*C*). As the magnitude of ε further increases, the folds increase in length, while wrinkles develop among and ahead of the folds (Movie S2). These results suggest that in contrast to conventional approaches, where the wrinkle-to-fold instability requires large compressive strains, in the presence of water the folding instability can be initiated using only small strains that are required to form wrinkles. In fact, when a droplet is placed on a skin prewrinkled by $\varepsilon \approx -0.01$, localized folds appear on the surface (Fig. S1).

To explain these observations, we briefly review the wrinkling of skin–substrate systems in the absence of a water droplet (21). For small compressive strains, the skin compresses together with the substrate, whereas for compressive strains beyond a critical strain ε_c, it is energetically more favorable for the skin to wrinkle, because thin elastic sheets are easier to bend than to compress. The characteristic wavelength λ_0 of wrinkles can be obtained by minimization of the total elastic energy, which consists of the bending energy of the skin (U_B) and the deformation energy of the substrate (U_D). For small strains, the height profile of the wrinkles can be approximated as $z(x) = A\cos(2\pi x/\lambda)$, where the amplitude $A = (\lambda/\pi)|\varepsilon|^{1/2}$ is obtained by assuming that the skin is incompressible.

Here, we introduce the in-plane dimensions of a rectangular-shaped soft substrate with a stiff skin of size $L_x \times L_y$ and bending stiffness $B = E_f h^3/12(1-\nu_f^2)$, where h, E_f, and ν_f are the thickness, Young's modulus, and Poisson's ratio of the skin, respectively. When the skin–substrate system is compressed in the x direction to the size $L_x(1-|\varepsilon|)$, we obtain $U_B = L_xL_y(4\pi^4/\lambda^4)BA^2 = L_xL_y(2\pi/\lambda)^2B|\varepsilon|$ and $U_D = L_xL_y(\pi/2\lambda)KA^2 = L_xL_y(\lambda/2\pi)K|\varepsilon|$. Note that the energy U_D is measured relative to the compressed state in the absence of wrinkles, and K is a constant given by $K = 2E_s(1-\nu_s)/(1+\nu_s)(3-4\nu_s)$, where E_s and ν_s are the Young's modulus and Poisson's ratio of the substrate, respectively. By minimizing the total energy $U_B + U_D$ with respect to λ, one obtains the characteristic wavelength of wrinkles $\lambda_0 = 2\pi(2B/K)^{1/3} \sim h(E_f/E_s)^{1/3}$. For moderate compressive strains, the wavelength is reduced to $\lambda = \lambda_0(1-|\varepsilon|)$, whereas for large compressive strains ($|\varepsilon| > 0.3$), sharp localized folds are observed due to nonlinear elastic deformations. As mentioned above, the onset of wrinkling occurs for compressive strains larger than $\varepsilon_c = -(Kh^3/16B)^{2/3} \sim -(E_s/E_f)^{2/3}$ or equivalently when the compressive stress in the skin reaches $\sigma_c = -3(BK^2/4h^3)^{1/3} \sim -(E_fE_s^2)^{1/3}$. In the wrinkled state, the compressive stress in the skin remains constant, $\sigma = (1/L_x L_x h)[d(U_B+U_D)/d\varepsilon] = \sigma_c$, as indicated by the linear relation of the energy costs U_B and U_D with ε. Thus, small additional surface forces can produce large deformations, which is critical for the explanation of our experimental results.

Extreme sensitivity of the wrinkled state to forces exerted by the liquid–air surface tension can be demonstrated as follows. The energy of the wrinkled state, which corresponds to the optimal wavelength of wrinkles λ_0, is $U_{wrinkled}(L_x, |\varepsilon|) = CL_xL_yB^{1/3}K^{2/3}|\varepsilon|$, where C is a numerical constant. When a liquid droplet is placed on the wrinkled surface, the liquid imbibes into certain wrinkled channels of total width L_1, whereas the rest of the wrinkles of total width $L_2 = L_x - L_1$ are free of liquid. The forces due to surface tension effectively compress the region L_1 to a new strain $|\varepsilon_1|$ by performing work $W = \gamma\cos\theta\, L_yL_1(|\varepsilon_1| - |\varepsilon|)$. Note that the effective strain $|\varepsilon_2|$ in the liquid-free region is subsequently

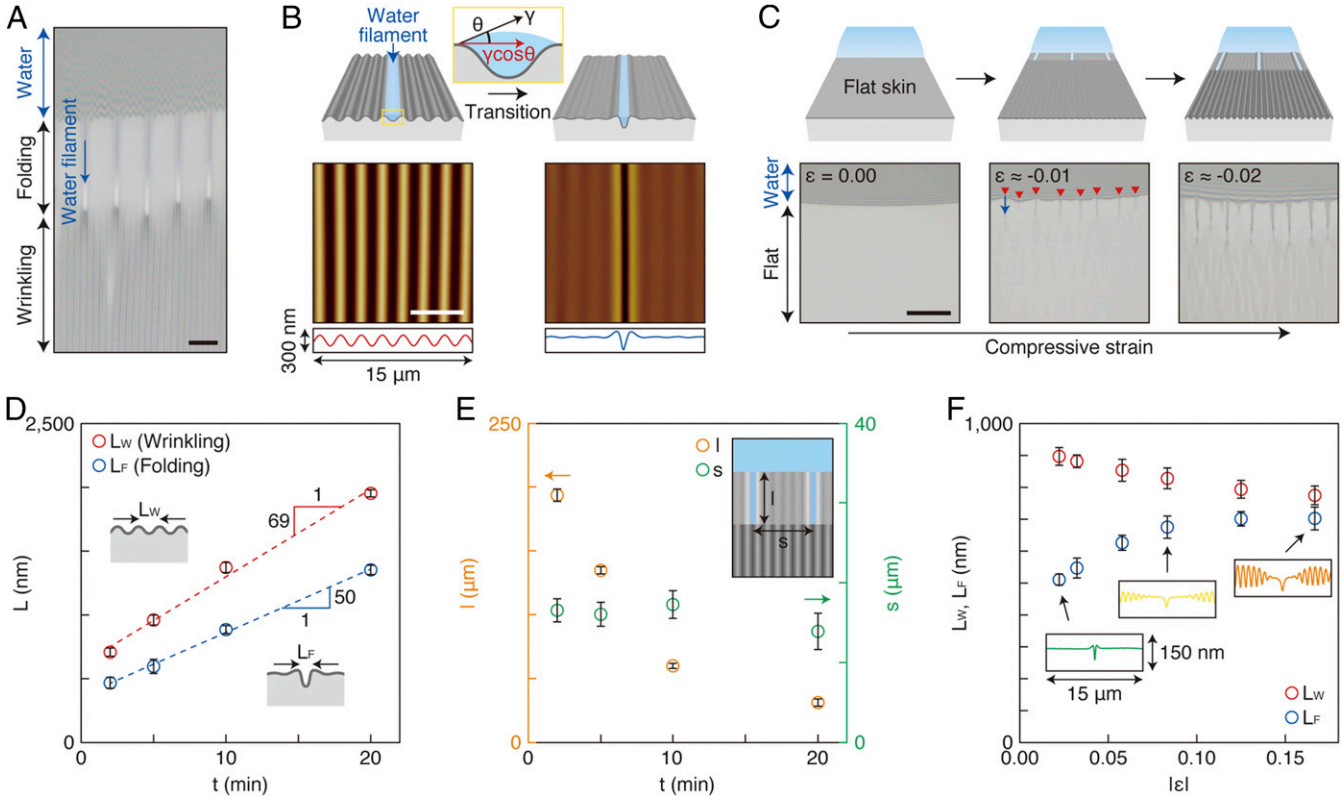

Fig. 2. Capillarity-induced skin folding. (*A*) Optical microscope image of an array of wrinkles and folds around the boundary of a water droplet placed on a wrinkled surface (t = 20 min, $\varepsilon \approx -0.03$). The blue arrow indicates a water filament. (*B*) Schematic illustrations of the wrinkle-to-fold transition of the skin due to surface tension forces of water. Representative AFM images and the line profiles are shown below the illustrations. (*C*) Schematic illustrations and optical microscope images showing the evolution of localized folds with increasing ε (t = 10 min). A water droplet was placed on the surface before compression; the blue arrow and red triangles indicate the formation of a water filament and localized folds, respectively. (*D* and *E*) The peak-to-peak distance of wrinkles (L_W) and folds (L_F) and the length (l) and spacing (s) of the folds as a function of t. (*E*, *Inset*) Schematic illustration showing the top view of an array of folds at the boundary. (*F*) L_W and L_F as a function of $|\varepsilon|$ (t = 3 min). (*F*, *Inset*) Line profiles of the folds for $|\varepsilon| \approx 0.02$, 0.08, and 0.17. (Scale bars: *A*, 10 μm; *B*, 5 μm; and *C*, 50 μm.)

reduced to $|\varepsilon_2| = |\varepsilon| - (|\varepsilon_1| - |\varepsilon|)(L_1/L_2)$ because the total width of the system is fixed to $L_x(1 - |\varepsilon|) = L_1(1 - |\varepsilon_1|) + L_2(1 - |\varepsilon_2|)$. The total free energy F is thus $F = U_{wrinkled}(L_1, |\varepsilon_1|) + U_{wrinkled}(L_2, |\varepsilon_2|) - W$. The relations presented above demonstrate that the elastic energy of the wrinkling is the same in both the initial and the final states [$U_{wrinkled}(L_x, |\varepsilon|) = U_{wrinkled}(L_1, |\varepsilon_1|) + U_{wrinkled}(L_2, |\varepsilon_2|)$]. Therefore, the total free energy of the wrinkled system can be lowered by increasing the compressive strain $|\varepsilon_1|$ of the wrinkled region that contains liquid, which is due to the work W done by the liquid–air surface tension. Note that in this linear elasticity analysis the total free energy would be minimized by making the compressive strain $|\varepsilon_1|$ of wrinkles containing liquid as large as possible. The surface tension thus keeps squeezing the wrinkled channels until the nonlinear elastic terms associated with sharp folds balance the capillary forces.

In our experimental system, $E_f = 200$ MPa, $E_s = 0.5$ MPa, $\nu_f = 0.35$, and $\nu_s = 0.5$ (23–26), yielding the critical compressive strain $\varepsilon_c \approx -0.01$ and critical compressive stress $\sigma_c \approx 2$ MPa; further, the skin thickness h increases linearly with the duration of oxygen plasma treatment t (27). Once a droplet is placed on the uncompressed surface ($\varepsilon = 0.00$), the stress in the skin of $h \approx 60$ nm due to the surface tension γ is approximately $\sigma \approx \gamma\cos\theta/h = 1$ MPa $< \sigma_c$. Thus, even with water, the surface should remain flat, as observed in our experiments (Fig. 2*C*). In contrast, once the skin is wrinkled, the water at the boundary of a droplet starts entering wrinkled channels, which are subsequently squeezed into folds by the capillary forces. As illustrated in Fig. 2*C*, when a droplet is placed on a flat skin–substrate surface, folding begins once the strain reaches the critical wrinkling strain $\varepsilon \approx \varepsilon_c \approx -0.01$. This experimental result suggests that wrinkles change into folds immediately after coming into contact with water, accompanied by the growth of water filaments. Such liquid filaments spontaneously form provided that the wetting angle θ for the surface falls below a critical value for a given aspect ratio (height/width) of wrinkles (28, 29), because, for large θ, water from the droplet does not enter wrinkled channels. As described above, the wrinkled skin is highly sensitive to additional surface forces, and the surface tension due to the filaments pulls in the skin until the force is balanced by nonlinear elastic deformations in the fold. As a result, the amplitude of the neighboring wrinkles is reduced (Fig. S2).

Next we characterize properties of the resulting array of folds. Fig. 2*D* summarizes the peak-to-peak distance of the wrinkles and folds, L_W and L_F, obtained at compressive strain $\varepsilon \approx -0.03$ for skins that were obtained by the oxygen plasma treatment for t = 2–20 min. Note that L_w is the same as the wavelength of wrinkles $\lambda = \lambda_0(1 - |\varepsilon|)$ introduced above, and L_F can be approximated as $L_F = \lambda_0(1 - |\varepsilon_F|) \sim h(E_f/E_s)^{1/3}(1 - |\varepsilon_F|)$ (15), where ε_F is the typical compressive strain for the folding transition of the skin–substrate system in the absence of water. We observe that L_w and L_F increase linearly with the duration of oxygen plasma treatment t, which is consistent with the equations above predicting linear scaling with the skin thickness h. When t = 2 min, for example, L_w and L_F measure 708 ± 32 and 467 ± 43 nm, respectively, which yield $L_F/L_W \approx 0.66$. Using $\varepsilon \approx -0.03$ and $\varepsilon_F \approx -0.35$, the latter of which is in the range of typical values of ε_F for the folding transition, the ratio $L_F/L_W \approx (1 - |\varepsilon_F|)/(1 - |\varepsilon|) \approx 0.67$, which is in good agreement with the

ENGINEERING

experimental data described above. Although the fold length l decreases with the duration of oxygen plasma treatment t, the spacing s between folds remains nearly constant (Fig. 2*E*). Because the effective bending resistance of the skin increases with the skin thickness h, which increases with t, we expect the fold length l to decrease with t. Fig. 2*F* reports L_w and L_F for t = 3 min as a function of $|\varepsilon|$, where representative line profiles of the folds for $|\varepsilon| \approx 0.02$, 0.08, and 0.17 are displayed. When $|\varepsilon|$ is small, the neighboring region of the fold appears almost flattened, which is probably because the amplitude of the initial wrinkles is small, and a larger number of wrinkles should be rearranged to accommodate the changes in local strain caused by water. However, for larger $|\varepsilon|$, the number of wrinkles involved in the formation of a single localized fold should become smaller. These results suggest that the initial strain affects the configuration of the resulting folds.

As mentioned above, once a localized fold is formed, the neighboring multiple wrinkles decrease their amplitude, which inhibits the formation of water filaments in the adjacent region, because water filaments only penetrate wrinkled channels with sufficiently large aspect ratio (height/width) (29). Therefore, the next wrinkle invaded by a water filament has to be some distance away, where the effects of the first fold are diminished. Because the aspect ratio of wrinkles A/L_w only depends on the compressive strain ε, we expect that the spacing s between folds should have no significant change with t (Fig. 2*E*). We observe that the wrinkle-to-fold transition occurs only upon the formation of water filaments, and the range of the contact angles where the transition occurs becomes slightly wider as h decreases (Fig. S3). One possible reason might be that for thinner skins the additional compressive stress imposed by water becomes more effective in altering the aspect ratio of the wrinkles around the boundary of the droplet, which affects the critical contact angle for water that imbibes into the wrinkled channels.

The aligned DNA nanowires confined to the folds appear on the surface when ε is properly adjusted (Fig. 3 *A* and *B*). The width of the nanowires can be manipulated by the dimensions of the initial wrinkles where a droplet is placed, which can be controlled by t and ε (Fig. 3 *C* and *D*). Note that by regulating the compressive/tensile strains we can also produce undulating DNA nanowires (Fig. 3*E*). Controlling the shape of nanowires is expected to yield unique electrical and optical properties, which could lead to the fabrication of new functional devices (30). However, the synthesis of shape-controlled nanowires generally relies on confinement-guided nanowire growth that requires prepatterned templates prepared by lithography-based methods, which are not readily available and hinder widespread applications. By virtue of strain engineering, our approach enables facile

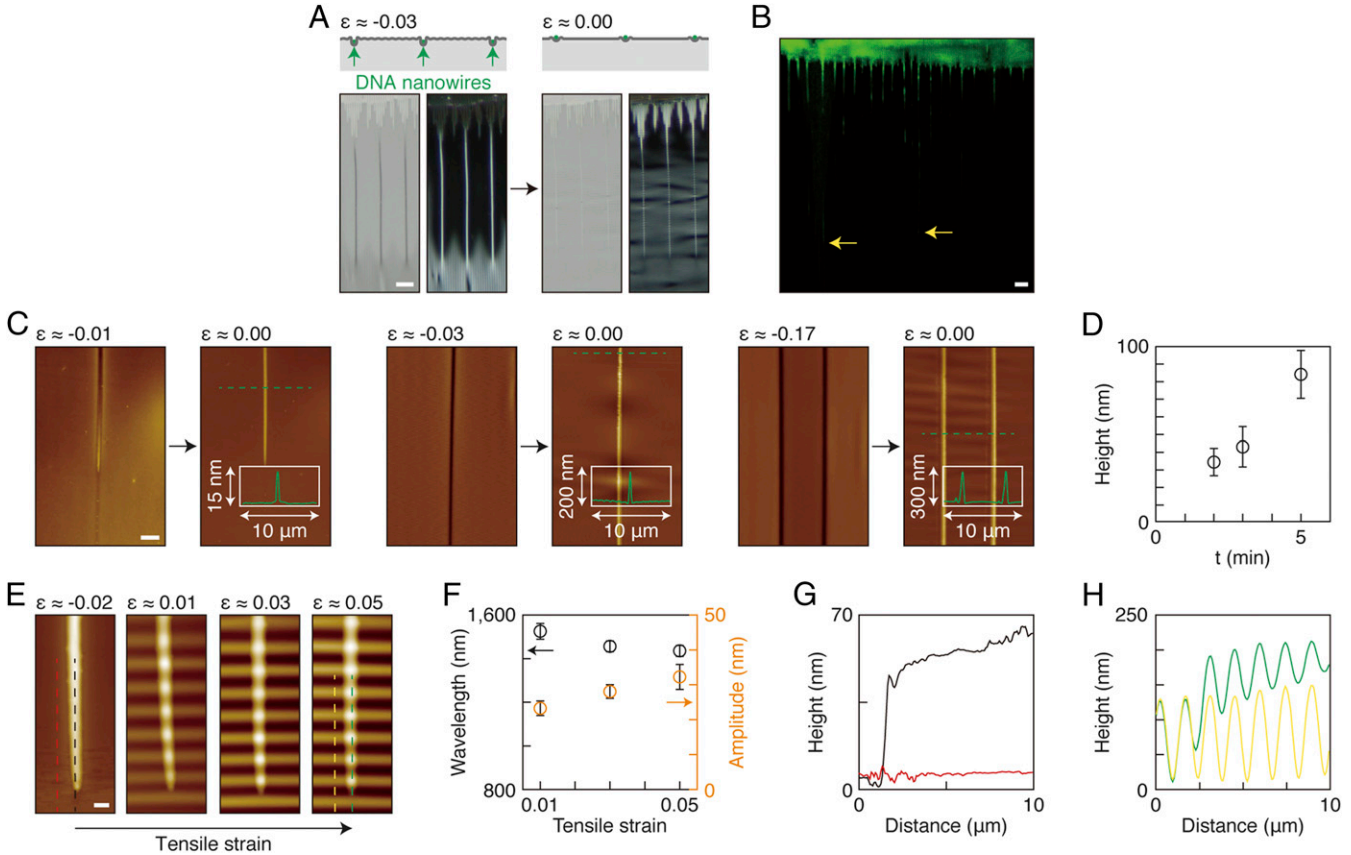

Fig. 3. Tunable DNA nanowires. (*A*) Bright- and dark-field optical microscope images of DNA nanowires created by the capillarity-induced wrinkle-to-fold transition. After evaporation of the droplet, the strain was adjusted to see the structure inside the folds. (*B*) Confocal microscope images of an array of DNA nanowires extending from the boundary to the locations indicated by the yellow triangles. (*C*) AFM images of DNA nanowires obtained using wrinkles prepared with various ε (t = 10 min). After the folds were formed, the strain was adjusted to $\varepsilon \approx 0.00$. The line profiles of the nanowires indicated by the green dotted lines are shown in the images. (*D*) Height of the nanowires as a function of t ($\varepsilon \approx -0.03$). (*E*) Changes in shape of a DNA nanowire from straight to wrinkled with an increase in tensile strain. (*F*) The wavelength (black symbols) and amplitude (orange symbols) of the wrinkled DNA nanowires as a function of applied tensile strain. (*G* and *H*) The line profiles of the DNA nanowire and the skin surface before and after application of the tensile strain (i.e., $\varepsilon \approx -0.02$ and 0.05, respectively). The color of the profiles corresponds to that of the dotted lines indicated in the AFM images shown in *E*. (Scale bars: *A* and *B*, 10 μm; *C*, 2 μm; and *E*, 1 μm.)

preparation of wrinkled DNA nanowires that could subsequently be used as a template for the synthesis of wavy metallic or semiconducting nanowires (Fig. 3 *E–H*), which would overcome the current limit.

We have uncovered a unique feature of the wrinkle-to-fold transition phenomenon of a skin–substrate system caused by capillary forces of water and demonstrated that this phenomenon yields a new route to the development of highly aligned DNA nanowires. Also, we have shown that this approach enables ready preparation of wrinkled DNA nanowires, which could make possible new fabrication opportunities for functional materials. Additional discussion of the effects of several parameters on the wrinkle-to-fold transition is provided in *Supporting Information* and Fig. S4–S10. Nonlinear analysis and modeling are required for improved quantitative understanding of the capillarity-induced wrinkle-to-fold transition. In addition, further studies may give insight into biological morphogenesis, because skin–substrate systems are ubiquitous in organisms where water is a major constituent.

Materials and Methods

Formation of Wrinkles and Folds. PDMS prepolymer was prepared by mixing a silicone elastomer base with a curing agent at a ratio of 20:1 by weight (Sylgard 184; Dow Corning Corp.). The mixture was cured at 70 °C for 2 h, and the resulting PDMS sheet with a thickness of 1.5 mm was cut into substrates of 10 × 30 mm. Before curing, the air bubbles trapped in the mixture were removed in a vacuum chamber. Each PDMS substrate was stretched uniaxially using a custom-built stretcher and treated with oxygen plasma for varying durations, t, with a low-pressure plasma system (COVANCE; Femto Science) to form a stiff oxidized skin of various thicknesses on the surface. The flow rate, power, and pressure during the treatment were maintained at 20 standard cm^3/min, 100 W, and ∼0.6 Torr, respectively. The stretch applied to the substrate was released to mechanically induce in the skin a nominal compressive strain ε, defined as the change in length per unit of the initial length of the substrate. The magnitude of the mechanical strain was controlled by adjustment of the level of the release of the stretch. A droplet of water (1–2 μL) was subsequently placed on the surface before or after application of the strain. Note that the experiments were generally performed right after oxygen plasma treatment to avoid the hydrophobic recovery of the surface because the surface hydrophilicity plays a key role in triggering the folding instability of the skin–substrate system, as discussed above.

DNA Molecules. λ-DNA (48,502 bp; 500 ng/μL in 10 mM Tris·HCl and 1 mM EDTA) was purchased from Bioneer Corporation. A droplet (1–2 μL) of the DNA solution [≤50 ng/μL in deionized (DI) water solution] was placed on wrinkled surfaces, followed by evaporation at room temperature. For the fluorescence measurement, λ-DNA was labeled at a dye:base pair ratio of 1:15. YOYO-1 iodide (3 μL; Life Technologies Corporation) was taken directly from the original solution and added to 8 ng/μL DNA solution (2.4 mL).

Surface Characterization. The surface morphology and DNA molecules were characterized with respect to ε using an atomic force microscope (AFM) (XE-70; Park Systems) and an optical microscope (BX53M; Olympus). The fluorescence measurements of the DNA molecules were performed in the dark using a confocal microscope (LSM 700; Zeiss). The wettability of the skin was evaluated by measurements of the static contact angles of droplets of distilled water (1 μL each) placed on the flat skin surface (i.e., ε = 0.00). The measurements were conducted using the sessile drop method, and changes in the wettability were characterized with respect to time after completion of the plasma treatment. The DNA nanowires formed in the folds were analyzed using the AFM. Note that after the folds containing DNA nanowires formed, the compressive strain that had been applied to the skin to create the initial wrinkles was removed or decreased so that the nanowires could appear on the surface.

ACKNOWLEDGMENTS. We thank Dr. Yong Lin Kong, Dr. François Boulogne, and Dr. Benedikt C. Sabass for helpful discussions. This work was supported by a Korea Institute of Science and Technology internal project, Grant MPSS-CG-2016-02 through the Disaster and Safety Management Institute funded by Ministry of Public Safety and Security of the Korean government, and National Research Foundation of Korea (NRF-2016M3C1B5906481 and CAMM-No. 2014063701).

1. Mao C, et al. (2004) Virus-based toolkit for the directed synthesis of magnetic and semiconducting nanowires. *Science* 303:213–217.
2. Nguyen K, et al. (2008) Synthesis of thin and highly conductive DNA-based palladium nanowires. *Adv Mater* 20:1099–1104.
3. Watson SMD, Pike AR, Pate J, Houlton A, Horrocks BR (2014) DNA-templated nanowires: Morphology and electrical conductivity. *Nanoscale* 6:4027–4037.
4. Catherall T, Huskisson D, McAdams S, Vijayaraghavan A (2014) Self-assembly of one dimensional DNA-templated structures. *J Mater Chem C Mater Opt Electron Devices* 2:6895–6920.
5. Michalet X, et al. (1997) Dynamic molecular combing: Stretching the whole human genome for high-resolution studies. *Science* 277:1518–1523.
6. Bensimon A, et al. (1994) Alignment and sensitive detection of DNA by a moving interface. *Science* 265:2096–2098.
7. Li B, et al. (2013) Macroscopic highly aligned DNA nanowires created by controlled evaporative self-assembly. *ACS Nano* 7:4326–4333.
8. Li B, Zhang C, Jiang B, Han W, Lin Z (2015) Flow-enabled self-assembly of large-scale aligned nanowires. *Angew Chem Int Ed Engl* 54:4250–4254.
9. Deen J, et al. (2015) Combing of genomic DNA from droplets containing picograms of material. *ACS Nano* 9:809–816.
10. Guan J, Lee LJ (2005) Generating highly ordered DNA nanostrand arrays. *Proc Natl Acad Sci USA* 102:18321–18325.
11. Charlot B, Teissier R, Drac M, Schwob E (2014) DNA on rails: Combing DNA fibers on nanogratings. *Appl Phys Lett* 105:243701.
12. De Angelis F, et al. (2011) Breaking the diffusion limit with super-hydrophobic delivery of molecules to plasmonic nanofocusing SERS structures. *Nat Photonics* 5:683–688.
13. Miele E, et al. (2015) Writing and functionalisation of suspended DNA nanowires on superhydrophobic pillar arrays. *Small* 11:134–140.
14. Wang QM, Zhao XH (2016) Beyond wrinkles: Multimodal surface instabilities for multifunctional patterning. *MRS Bull* 41:115–122.
15. Sun JY, Xia SM, Moon MW, Oh KH, Kim KS (2012) Folding wrinkles of a thin stiff layer on a soft substrate. *Proc R Soc A* 468:932–953.
16. Kim JB, et al. (2012) Wrinkles and deep folds as photonic structures in photovoltaics. *Nat Photonics* 6:327–332.
17. Nagashima S, Ebrahimi H, Lee KR, Vaziri A, Moon MW (2015) Tunable nanochannels fabricated by mechanical wrinkling/folding of a stiff skin on a soft polymer. *Adv Mater Interfaces* 2:1400493.
18. Kim P, Abkarian M, Stone HA (2011) Hierarchical folding of elastic membranes under biaxial compressive stress. *Nat Mater* 10:952–957.
19. Tallinen T, Biggins JS (2015) Mechanics of invagination and folding: Hybridized instabilities when one soft tissue grows on another. *Phys Rev E Stat Nonlin Soft Matter Phys* 92:022720.
20. Tallinen T, et al. (2016) On the growth and form of cortical convolutions. *Nat Phys* 12:588–593.
21. Brau F, et al. (2011) Multiple-length-scale elastic instability mimics parametric resonance of nonlinear oscillators. *Nat Phys* 7:56–60.
22. Wang Q, Zhao X (2015) A three-dimensional phase diagram of growth-induced surface instabilities. *Sci Rep* 5:8887.
23. Cerda E, Mahadevan L (2003) Geometry and physics of wrinkling. *Phys Rev Lett* 90:074302.
24. Pocivavsek L, et al. (2008) Stress and fold localization in thin elastic membranes. *Science* 320:912–916.
25. Hillborg H, Gedde UW (2012) Oxidative surface treatment of silicone rubber. *Silicone Surface Science*. Advances in Silicon Science, eds Owen MJ, Dvornic PR (Springer, Dordrecht, The Netherlands), Vol 4, pp 299–315.
26. Wang ZX, Volinsky AA, Gallant ND (2014) Crosslinking effect on polydimethylsiloxane elastic modulus measured by custom-built compression instrument. *J Appl Polym Sci* 131:41050.
27. Moon MW, Vaziri A (2009) Surface modification of polymers using a multi-step plasma treatment. *Scr Mater* 60:44–47.
28. Khare K, Zhou J, Yang S (2009) Tunable open-channel microfluidics on soft poly(dimethylsiloxane) (PDMS) substrates with sinusoidal grooves. *Langmuir* 25:12794–12799.
29. Ohzono T, Monobe H, Shiokawa K, Fujiwara M, Shimizu Y (2009) Shaping liquid on a micrometre scale using microwrinkles as deformable open channel capillaries. *Soft Matter* 5:4658–4664.
30. Pevzner A, et al. (2012) Confinement-guided shaping of semiconductor nanowires and nanoribbons: "Writing with nanowires". *Nano Lett* 12:7–12.
31. Bowden N, Brittain S, Evans AG, Hutchinson JW, Whitesides GM (1998) Spontaneous formation of ordered structures in thin films of metals supported on an elastomeric polymer. *Nature* 393:146–149.
32. Lee JN, Park C, Whitesides GM (2003) Solvent compatibility of poly(dimethylsiloxane)-based microfluidic devices. *Anal Chem* 75:6544–6554.
33. Toga KB, Huang J, Cunningham K, Russell TP, Menon N (2013) A drop on a floating sheet: Boundary conditions, topography and formation of wrinkles. *Soft Matter* 9:8289–8296.

Supporting Information

Nagashima et al. 10.1073/pnas.1700003114

Folds Formed with Small Strains

Figs. S1 and S2 present microscope images of localized folds formed using wrinkles prepared with $\varepsilon \approx -0.01$ and -0.03, respectively. For Fig. S2, the bottom surface has roughness whose mean height is around 1 nm, which can be attributed to the inherent surface morphology of the PDMS substrate because such a structure is present on the flat skin as well.

Wettability and Thickness of the Skin

Fig. S3*A* shows a diagram of the wrinkle-to-fold transition for various t and θ. As t increases, the range of θ that allows for the transition becomes smaller. Note that θ was controlled by exploiting an aging effect of the plasma-treated hydrophilic skin. This effect is a well-known phenomenon that if a plasma-treated hydrophilic surface is left in contact with air, the surface changes to hydrophobic over time to lower the surface free energy through rearrangements of polar groups on the surface and/or attachment of contaminants to the surface. Thus, different values of θ were obtained by varying when to place a water droplet on a wrinkled surface after completion of the oxygen plasma treatment. Fig. S3 *B* and *C* shows optical and atomic force microscope images of a wrinkled surface prepared using $\varepsilon \approx -0.03$ and t = 30 min obtained, respectively, before and after evaporation of a water droplet placed on the surface, which demonstrates the suppression of the wrinkle-to-fold transition. The thickness of the skin is estimated to be 112 nm using $h \approx L_W(E_s/E_f)^{1/3}/4.4$ (31), which is about twice the thickness for t = 10 min where the transition occurs.

Young's Modulus

As described in the main text, the Young's modulus of the substrate affects the response of the skin attached to the substrate. Fig. S4 presents optical and atomic force microscope images showing the wrinkle-to-fold transition at the boundary for E_s = 2 and 0.5 MPa, respectively. The Young's moduli were controlled by adjustment of the mixture ratio of a silicone elastomer base with a curing agent at ratios of 10:1 and 20:1 by weight, respectively. As the Young's modulus increases, *l* and *s* decrease.

Swelling

Fig. S5 presents optical and atomic force microscope images of the flat surface obtained before and after evaporation of a water droplet placed on the surface, respectively, where no wrinkles or folds are observed. These results indicate that even if the skin swells, the strain induced in the skin should be below a critical level. Therefore, the effect of swelling on the wrinkle-to-fold transition is negligible. With respect to the PDMS substrate, Lee et al. (32) investigated the swelling of PDMS in various solvents and concluded that water does not swell PDMS.

Fig. S6 shows bright- and dark-field optical microscope images of a water droplet placed on a wrinkled surface. In the dark-field image, we observe the folds developing around the boundary of the droplet, whereas in the region beneath the droplet that is away from the boundary we only see the wrinkles that have been formed before deposition of the droplet. Note that there is a region where folds invade inward from the boundary of the droplet as indicated by the orange dotted box. Such an invasion of the patterns from outside to inside the droplet can be attributed to the boundary confinement (33).

Laplace Pressure

The vertical force acting downward (F_d) due to the Laplace pressure is given by $F_d \approx p\pi R^2$, where R is the radius of the droplet, and the vertical component of the capillary force upward at the contact line (F_u) is written as $F_u = 2\pi R\gamma\sin\theta$ (Fig. S7). Because these forces are balanced, $p = 2\gamma\sin\theta/R$. The strain in the vertical direction, ε, can be expressed by $\varepsilon \approx p/E_f = 2\gamma\sin\theta/(RE_f)$. Using values of $\gamma = 0.072$ N/m, R = 2 mm, E_f = 200 MPa, and $\theta \approx 5°$, the strain is calculated to be $\varepsilon \approx 10^{-7}$, which is so small that the effect of the Laplace pressure inside the droplet of water is negligible.

DNA Molecules

Spontaneous evaporation of a droplet of the DNA solution on an Si wafer results in the formation of coiled DNA molecules whose contour length is 16.3 μm (Fig. S8*A*). When a droplet of the DNA solution is placed on the flat surface, the molecules tend to accumulate at the contact line, known as the coffee-ring effect, leading to suppression of the development of an array of folds at the boundary even though compressive strain is incrementally applied to the skin (Fig. S8*B*). This experimental observation implies that there would be other factors, including the concentration of the DNA solution, that allow for proper development of the folds at the boundary, details of which remain to be studied.

We have performed several sets of experiments to investigate the effect of DNA concentration on the wrinkle-to-fold transition by using DNA solutions of concentrations ranging from 8 to 500 ng/μL (Figs. S9 and S10). First, we measured contact angles of droplets on a pristine flat PDMS substrate to see the tendency of contact angle changes for a wide range of concentration (open circles in Fig. S9). When the concentration is up to 50 ng/μL, the contact angle reaches ∼120°. Further increase in concentration to 250–500 ng/μL leads to an increase in contact angle to ∼130°. These results imply that the surface tension would slightly change according to the range of concentration. Next, based on the aforementioned results, we performed another set of contact angle measurements by using a plasma-treated hydrophilic PDMS substrate for DI water and DNA solutions (50 and 500 ng/μL), whose results are presented by the filled circles in Fig. S9. The contact angle increased from ∼4° to ∼15° as the concentration increased from 0 to 500 ng/μL.

When a droplet of DNA solution of 50 ng/μL was placed on a wrinkled surface, the wrinkle-to-fold transition occurred, forming DNA nanowires, whereas that of 500 ng/μL inhibited the transition, and the accumulation of the molecules was observed at the boundary (Fig. S10). Here, we revisit Fig. S3*A* presenting the conditions of t and θ under which the wrinkle-to-fold transition occurs. The DNA solutions of 50 and 500 ng/μL have $\theta \approx 10°$ and 15°, yielding $\cos\theta \approx 0.985$ and 0.966, respectively. According to Fig. S3*A*, the latter value is in the range where the transition does not occur, which is in agreement with the experimental observation shown in Fig. S10. These results suggest that the surface tension and contact angle play important roles in triggering the wrinkle-to-fold transition and forming DNA nanowires. Further detailed investigations would be needed to elucidate the underlying physics and to find various applications of our system.

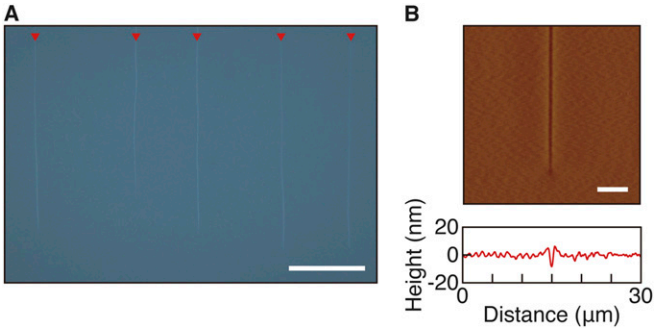

Fig. S1. Folds formed with a small strain. (*A*) Optical and (*B*) atomic force microscope images of folds formed by $\varepsilon \approx -0.01$ (t = 10 min). The red triangles indicate the folds. (Scale bars: *A*, 50 μm and *B*, 5 μm.)

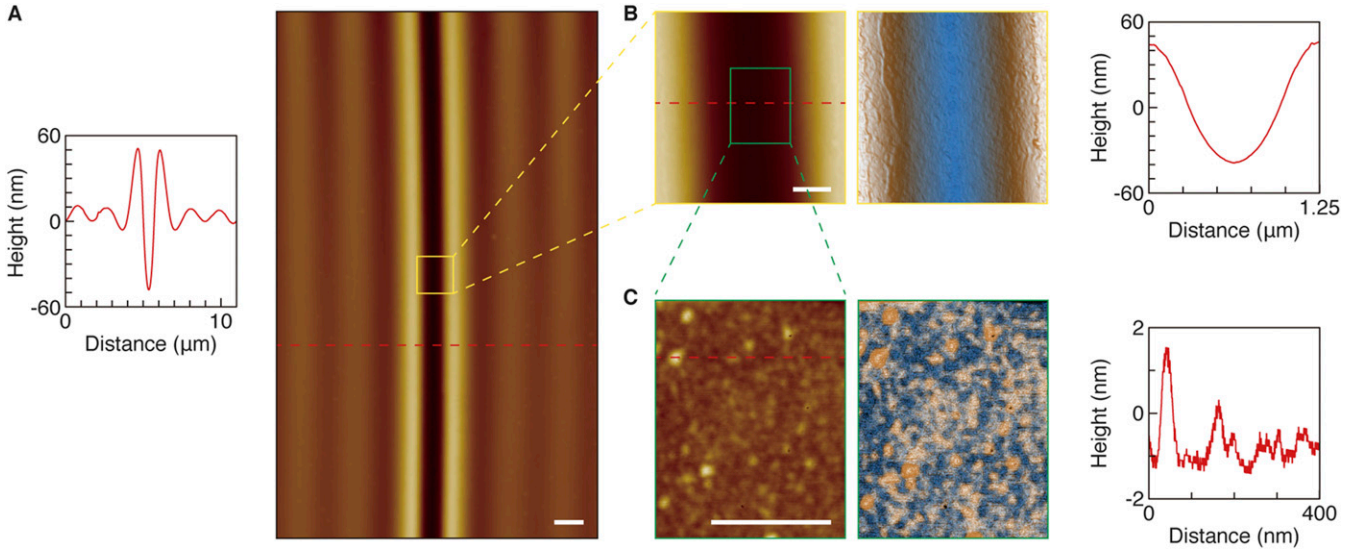

Fig. S2. Surface morphology of a fold. (*A*–*C*) AFM images of a fold appearing on a wrinkled surface (t = 20 min, $\varepsilon \approx -0.03$). (Scale bars: *A*, 1 μm; *B* and *C*, 250 nm.)

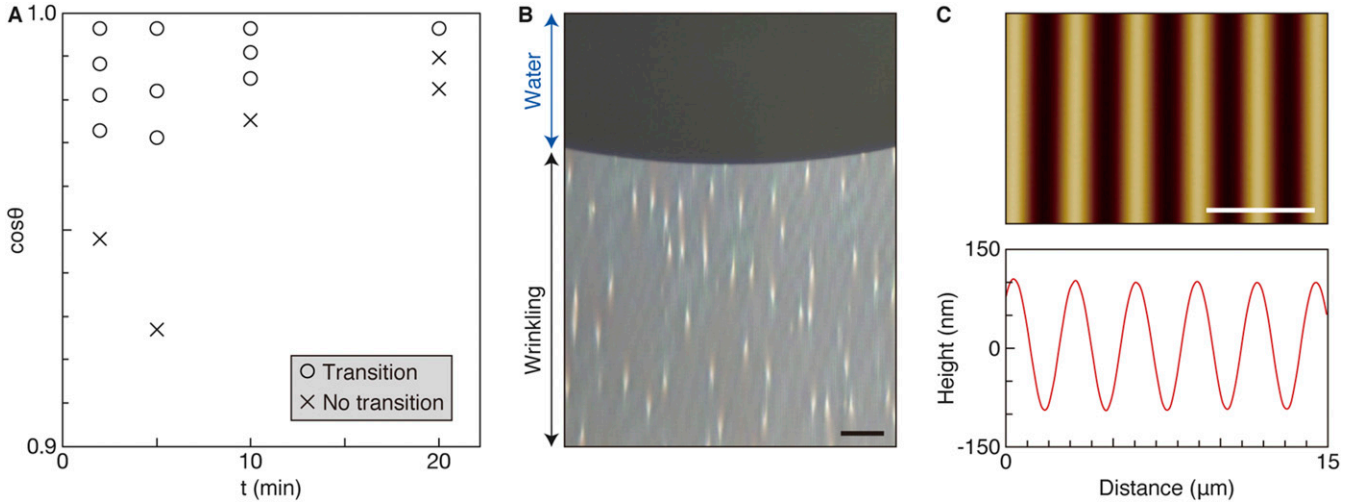

Fig. S3. Inhibition of the wrinkle-to-fold transition. (*A*) Diagram of the wrinkle-to-fold transition for various t and θ ($\varepsilon \approx -0.03$). (*B* and *C*) Optical and atomic force microscope images of the surface morphology around the boundary of the droplet of water placed on the wrinkled surface (t = 30 min), demonstrating the inhibition of the transition. (Scale bars: *B*, 50 μm and *C*, 5 μm.)

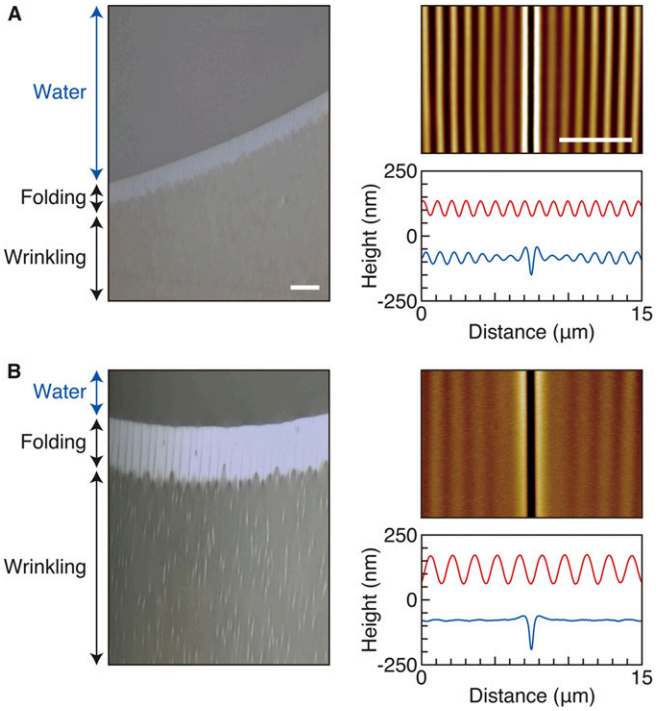

Fig. S4. Effect of the elastic modulus of the PDMS substrates. Surface morphological changes around the contact line of a droplet placed on wrinkled surfaces prepared with different mixture ratios of PDMS: (*A*) 10:1 and (*B*) 20:1 (t = 10 min, $\varepsilon \approx -0.03$). Each optical microscope image was taken when the droplet was on the wrinkled surface, and the AFM images and the corresponding line profiles were obtained after evaporation of the droplet. The red and blue lines present the profiles of the wrinkles and the folds, respectively. (Scale bars in the optical and atomic force microscope images, 50 and 5 μm, respectively.)

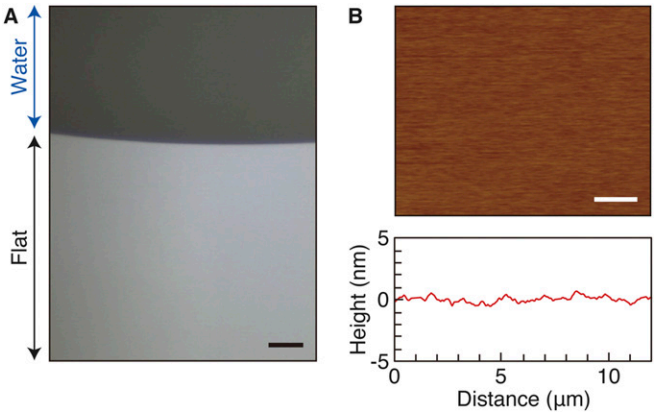

Fig. S5. Surface morphology of the hydrophilic skin in the uncompressed state. (*A*) Optical microscope image of the surface on which a droplet of water is sitting. (*B*) AFM image of a region nearby the boundary of the droplet and its corresponding line profile. This image was obtained after evaporation of the droplet. (Scale bars: *A*, 50 μm and *B*, 2 μm.)

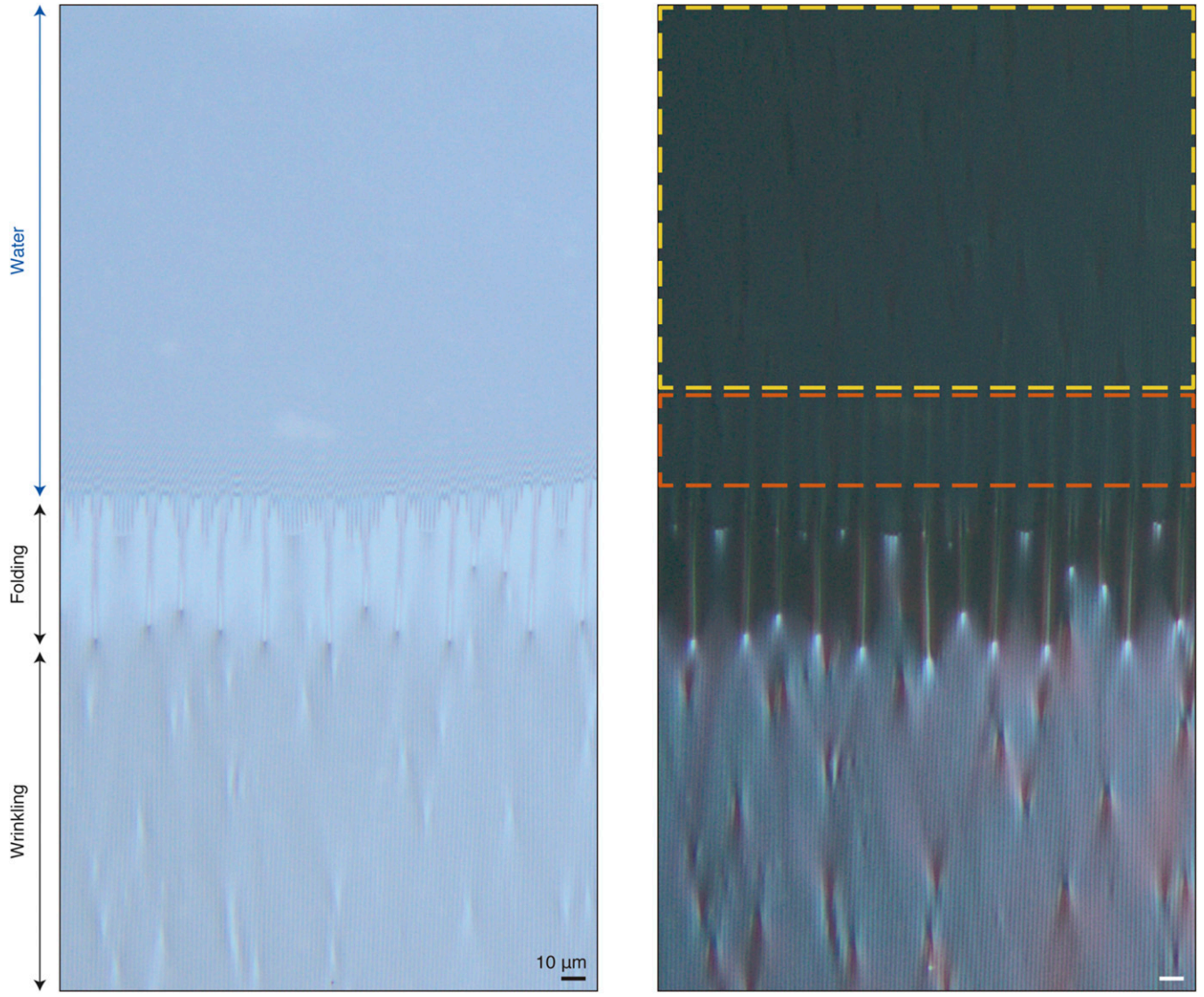

Fig. S6. Folds developing around the boundary of a droplet. Bright-field (*Left*) and dark-field (*Right*) optical microscope images of a droplet placed on a wrinkled surface (t = 20 min, $\varepsilon \approx -0.03$) are presented. These images were obtained as soon as the droplet started receding from the boundary. The region indicated by the orange dotted box illustrates the development of folds around the boundary under the droplet, and the area beneath the droplet indicated by the yellow one shows wrinkles that were created before deposition of the droplet.

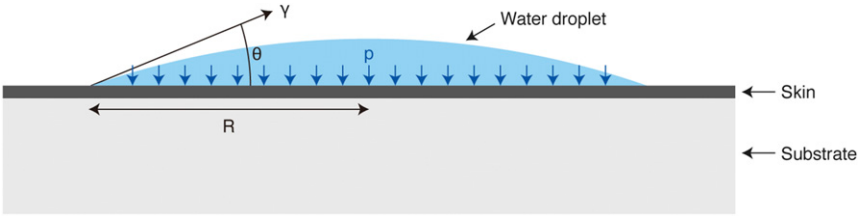

Fig. S7. Schematic illustration of a droplet sitting on the skin–substrate system. The droplet of water whose surface tension is ε has a radius of R, and its contact angle is θ. The Laplace pressure inside the droplet, p, is normal to the surface of the skin–substrate system.

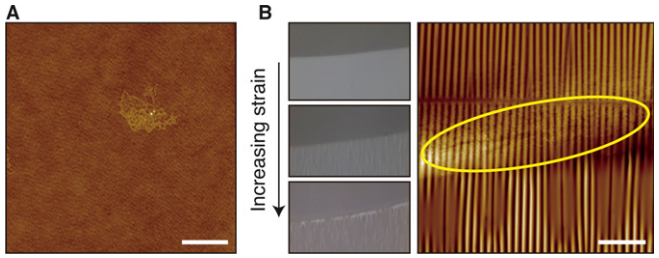

Fig. S8. AFM images of λ-DNA. (*A*) Coiled DNA molecules on an Si wafer. (*B*) A droplet of the DNA solution (8 μg/mL) was placed on the flat skin, and compressive strain was subsequently induced in the skin. Sequential optical microscope images on the left depict suppressed development of folds around the boundary due to the coffee-ring effect, as illustrated in the AFM image on the right (the yellow ellipse). (Scale bars: *A*, 1 μm and *B*, 10 μm.)

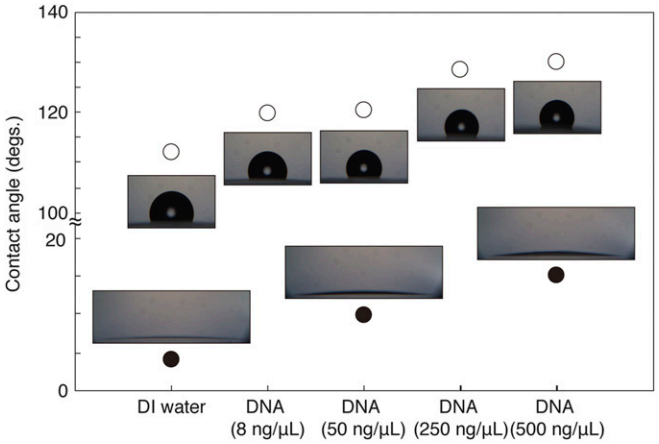

Fig. S9. Effect of the DNA concentration on the contact angle of a droplet. A droplet (1 μL) of various concentrations of the DNA solution was placed on a pristine or oxygen-plasma-treated flat PDMS substrate, and the results are presented by ○ and ●, respectively.

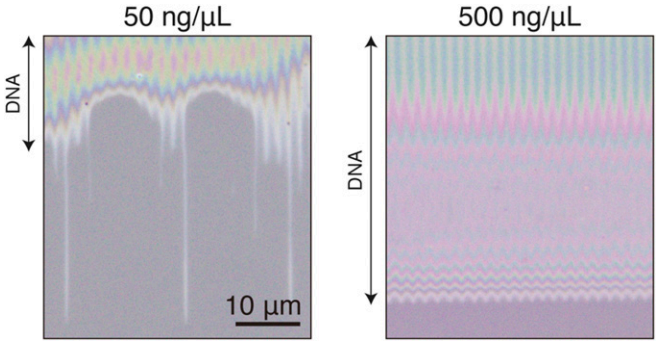

Fig. S10. Effect of the DNA concentration on the wrinkle-to-fold transition. A droplet (1 μL) of water containing different concentrations (50 and 500 ng/μL) of DNA molecules was placed on a wrinkled surface (t = 10 min, $\varepsilon \approx -0.03$). The optical microscope images illustrate the development of folds for 50 ng/μL (*Left*) and the suppression for 500 ng/μL (*Right*).

Movie S1. Instantaneous wrinkle-to-fold transition. This movie shows the wrinkle-to-fold transition that instantaneously occurs upon deposition of a water droplet on a wrinkled surface (t = 2 min, $\varepsilon \approx -0.03$). The folded region can be seen ahead of the droplet spreading over the surface.

Movie S1

Movie S2. Emergence and growth of localized folds. This movie shows the emergence and growth of localized folds with increasing strain. A water droplet was placed on the flat skin surface, and compressive strain was incrementally applied (t = 10 min). This movie plays at three times real-time speed.

Movie S2